RSC Advances

PAPER

View Article Online
View Journal | View Issue

Cite this: *RSC Adv.*, 2022, **12**, 28254

Anisotropic hydrogel fabricated by controlled diffusion as a bio-scaffold for the regeneration of cartilage injury†

Xiaotian Yu,‡[abc] Zhantao Deng,‡[a] Han Li,‡[ab] Yuanchen Ma,[a] Xibo Ma[cd] and Qiujian Zheng *[ae]

Controlled fabrication of anisotropic materials has become a hotspot in materials science, particularly biomaterials, since the next generation of tissue engineering is based on the application of heterogeneous structures that can simulate the original biological complexity of the body. The current fabrication method of producing anisotropic materials involves expensive and highly specialized equipment, and not every conventional method can be applied to preparing anisotropic materials for corresponding tissue engineering. Anisotropic materials can be easily applied to a problem in tissue engineering: cartilage injury repairing. The articular cartilage consists of four spatially distinct regions: superficial, transitional, deep, and calcified. Each region has a specific extracellular matrix composition, mechanical properties, and cellular organization; this calls for the application of an anisotropic hydrogel. Controlled diffusion, under the assistance of buoyancy, has been considered a generalized method to prepare materials using a gradient. The diffusion of two solutions can be controlled through the difference in their densities. In addition to providing anisotropy, this method realizes the *in situ* formation of an anisotropic hydrogel, and simplifies the preparation process, freeing it from the need for expensive equipment such as 3D printing and microfluidics. Herein, an anisotropic hydrogel based on a decellularized extracellular matrix is fabricated and characterized. The as-prepared scaffold possessed specific chemical composition, physical properties, and physiological factor gradient. *In vitro* experiments ensured its biocompatibility and biological effectiveness; further *in vivo* experiments confirmed its application in the effective regeneration of cartilage injury.

Received 17th August 2022
Accepted 22nd September 2022

DOI: 10.1039/d2ra05141a

rsc.li/rsc-advances

1 Introduction

The knee-joint is one of the most complex joints in the human body, consisting of the femur, tibia, patella, meniscus, ligament, *etc.*, and plays a comprehensive and complex stabilizing role in the normal physiological activities of the human body and has a greater risk of injury. In recent years, with the further popularization of national fitness and the gradual aging of the population in China, knee joint diseases also show a straight-rise trend. Cartilage injury can lead to degenerative disease with joint pain, effusion, and dysfunction as the primary clinical manifestations. Without timely intervention, it will lead to traumatic arthritis, further affecting the patient's activity and function. Articular cartilage mainly relies on articular fluid to provide nutrition. It has the characteristics of no blood supply and nerve distribution, and its self-repair ability is weak. In addition, fibrocartilage is usually available instead of hyaline cartilage. Because of its high tensile and low compressive modulus, it is easy to harden the damaged part if used to replace the original hyaline cartilage.

Currently, the treatment methods for cartilage injury are mainly divided into two categories: drug therapy and surgery. Standard clinical therapies have some limitations; for example, autologous cartilage transplantation requires limited sources of cartilage; Allogeneic cartilage transplantation is easy to induce an immune response; the therapeutic effect of periosteal transplantation is not stable. Arthroscopic cleaning and debridement could not repair the damaged cartilage. Bone marrow stimulation is ineffective in patients who are less able to repair themselves. Advanced patients usually need an artificial joint replacement, which may lead to postoperative complications and recurrence. Moreover, the service life of

[a]*Department of Orthopedics, Guangdong Provincial People's Hospital, Guangdong Academy of Medical Sciences, China. E-mail: zhengqiujian@gdph.org.cn*
[b]*Guangdong Cardiovascular Institute, Guangzhou, Guangdong, China*
[c]*CBSR&NLPR, Institute of Automation, Chinese Academy of Sciences, Beijing, China*
[d]*School of Artificial Intelligence, University of Chinese Academy of Sciences, Beijing, China*
[e]*The Second School of Clinical Medicine, Southern Medical University, China*

† Electronic supplementary information (ESI) available. See https://doi.org/10.1039/d2ra05141a

‡ These author contributed equally to the work.

artificial joints is limited, and revision surgery is complicated and risky, which may cause secondary injuries to patients.[1]

Traditional medical therapies for cartilage damage mainly use sodium hyaluronate and dexamethasone for interarticular injections, which are effective in relieving pain and improving joint mobility due to their anti-inflammatory and lubricating properties. However, they are not effective in repairing cartilage. Moreover, the primary intervention method is intra-articular injection. Due to the lack of specificity of drugs, it is not easy to be absorbed in the injured site. In contrast, the drugs that are not absorbed will be degraded due to the presence of relevant enzymes or will be separated from the site of action with the metabolism of synovial fluid, resulting in a short time of action. Long-term injection of these drugs into joints can cause side effects such as calcification of the joint capsule, skin atrophy, and loss of cartilage volume, and can even cause systemic adverse reactions such as transient hyperglycemia, cushing-like syndrome, or skin flushing.[2]

Below the surface of the joint, articular cartilage is divided into the following layers: superficial, intermediate, deep, and calcified cartilage. The types, morphology, arrangement of collagen fibers, mechanical properties, and microstructure of chondrocytes were different in other regions. Traditional tissue engineering scaffolds are difficult to repair cartilage with different degrees of damage due to their shortcomings of single component and poor mechanical properties. Although bi-layer and multi-layer scaffold materials have been developed for the integrated repair of damaged cartilage, such scaffolds cannot simulate the multilayer structure of cartilage itself. The appearance of multilayer scaffolds further improves the repair efficiency of damaged cartilage. However, there are interfaces between different layers, which may fall off due to poor fixation. Therefore, the preparation of *in situ* formed anisotropic scaffold materials can better simulate the original biological characteristics of cartilage tissue and play a good repair effect.

In nature, gradients play a crucial role in various tissues' structural composition and physiological function, including cartilage and tendons.[3–6] These natural gradients must be reconstructed in the design of tissue-engineered scaffolds to prepare fully functional biological scaffolds. In doing so, consideration must be given to the various gradients present in natural tissues, including chemical composition (for instance, extracellular matrix and growth factors), physical properties (for instance, stiffness and morphology) and biological factors. These gradient properties regulate the morphology and behavior of local cells through their spatial distribution and play an essential role in tissue reconstruction.[7–9] Therefore, designing materials with different gradients are the focus of current tissue engineering research. Current research results show that anisotropic materials are manufactured using multichannel microfluidic devices or 3D printing.[10–12] However, these methods require specialized equipment and are often limited by specific properties, such as viscosity or gelation dynamics. Methods such as optical patterning and magnetic field control are also used to generate gradients. However, these preparation methods also impose more inherent requirements on the material's reactivity (optical/magnetic).[13] A general synthesis method that can be applied to common materials remains to be explored until the application of buoyancy to material preparation becomes apparent.

Buoyancy is a standard parameter used in stabilizing the formation of sucrose gradients for cell and organelle fractionation.[14,15] This method has been further used to separate nanoparticles with density-gradient organic solvents.[16] However, there is only few numbers of research use buoyancy to synthesize anisotropic materials. For example, Parameswaran and Shukla proposed a system in which cenosphere (hollow silica-alumina particles) are floated on top of the polyester resin, and the structure is subsequently fixed in a solid matrix after 18 hours of curing process. Resulting in a polymer material possessing a chemical component gradient and mechanical gradient.[17] Similarly, Bierce and Thompson showed that gas injected into a molten aluminum alloy could disperse into tiny particle stable bubbles when mixed. These bubbles form liquid foam at the top of the melt and then cool to form metallic structures with porosity gradients.[18]

The gradient formed by the injection of one fluid material into another can be fixed by fast gelation or polymerization. This strategy could be used to prepare materials with a variety of gradient properties such as chemical composition, mechanical properties, and biochemical curves from various raw materials (gelatine methylacrylyl, agarose, chitosan, and acrylate polymers). The universality and simplicity of this preparation strategy can inspire a lot in the manufacturing and application of composite material in tissue engineering.

Decellularized extracellular matrix (dECM) -based biomaterials for cartilage injury repair are receiving increasing attention, especially for the elderly and athletes. However, conventional dECM stents are poorly infiltrated and are usually surgically implanted. In order to overcome these limitations, we first decellularized the knee cartilage of pigs by chemical, physical and biological methods. We then further digested it with protease to develop an injectable dECM pre-gel solution that can be injected into the defect site through a syringe and realized *in situ* self-gelation in a physiological environment. This articular cartilage-derived dECM hydrogel with adjustable compression and initial modulus is an ideal material for preparing tissue-engineered scaffolds for repairing cartilage damage. Hydrogels can promote cell infiltration and show good biocompatibility in the *in vitro* culture of bone marrow mesenchymal stem cells. After 14 days of culture, ECM hydrogels showed good biocompatibility. These preliminary experimental results indicate that the designed injectable dECM anisotropic hydrogel has excellent potential for the repair and regeneration of articular cartilage injury.

There is increasing interest in using biomaterials to simulate natural tissue microenvironments, as scaffolds and replacements for tissue regeneration can be provided in a similar environment to the original tissue.[19] One approach is utilizing decellularized extracellular matrix (dECM) scaffold through the decellularization of natural tissues. Scaffolds fabricated this way contain components similar to the tissue's original ECM and show attractive biological activity for tissue repair and regeneration.[20] Cell membrane antigens and nuclear

components can be removed through decellularization techniques to eliminate immune responses and construct a suitable microenvironment for cell proliferation to promote the formation of new tissues. Making tissue-specific dECM a promising reagent in the repairment and regeneration of specific tissues and organs. For example, decellularized porcine submucosal (SIS) materials have been commercialized and used clinically for skeletal muscle therapy.[21,22] Heart-derived dECM materials were implanted into infarcted hearts to promote endogenous cardiomyocyte recruitment and restore cardiac function.[23] Porcine meniscal-derived acellular scaffolds have also been used with primary cells and stem cells to promote meniscal regeneration.[24] Rat meniscus-derived scaffolds inoculated with MSCs were implanted into the meniscus of rats with the defective meniscus, which showed better cartilage protection than conventional meniscectomy.[25]

The decellularized ECM scaffold still maintains the solid appearance of form tissue. To accomplish the target of *in situ* gelation, the bulk dECM could be processed into injectable hydrogels after further digestion. The cells could easily be loaded into evenly distributed hydrogels to fill irregularly shaped defects. In addition, injectable hydrogels are directly injected into the site of cartilage injury in combination with minimally invasive arthroscopy, which is popular in clinics.[26] In contrast, ECM stents usually require incision surgery, and continuous movement may cause the stent to detach from the implanted site. Injectable hydrogels have been reported from the heart,[27] dermis,[28] bone,[29] bladder,[30] liver,[31] nervous system,[32] blood vessels[33] and brain[34]. It is worth noting that porcine heart-derived hydrogels are delivered through catheters to porcine infarcted hearts, which shows great clinical promise. However, no studies have been reported on injectable *in situ* formed anisotropic hydrogels to repair cartilage damage, which is the focus of this study.

In this study, we processed porcine knee cartilage into a pre-gel solution by decellularization and enzyme digestion and constructed the anisotropic using the buoyancy method. The pre-gel solution can complete gelation under mild conditions and fix the original gradient properties. We loaded kartogenin (KGN) drug carrier and bone marrow mesenchymal stem cells into the hydrogel, and studied the biosafety and effectiveness of the hydrogel. The major components of the acellular matrix (collagen and glycosaminoglycan (GAG)), gel dynamics, and mechanical properties of hydrogels were measured. The gradient properties of mechanical properties and biological factors were also characterized. Finally, rabbits were chosen as an animal model to evaluate the performance of hydrogel in cartilage repair.

2 Experiment

2.1 Preparation of decellularized extracellular matrix

Cartilage tissue was cut into 1 mm thick slices, frozen at −80 °C, and grounded into a coarse powder. 1 g powder was dispersed in 500 mL 1% SDS/PBS solution and stirred for 72 h. The SDS solution was replaced every 24 h. Subsequently, the samples were dispersed in 500 mL 0.1% EDTA/PBS solution for 24 h and last overnight in large amounts of deionized water to remove residual chemicals. Finally, the resulting dECM was frozen, stored at −80 °C, and continued to lyophilized. Finally, ground to a fine powder and stored at −20 °C for future usage. Enment was performed using OCT embedding at −20 °C and subsequently cut into 7 mm thick sections for hematoxylin/eosin and DAPI staining. A fluorescence inverted microscope was used to observe the staining results, and a scanning electron microscope was used to observe the dECM morphology.

2.2 Characterization of acellular matrix DNA content

Prepared dECM was further digested using a HCl (0.01 M) solution of pepsin (1 mg mL^{-1}), for a typical procedure, 1 g of dECM was dispersed in 100 mL pepsin solution, and the residual was subsequently removed by a centrifuge. The upper-layer solution was centrifuged for 30 min at 10 000 g in a phenol/chloroform/isovalyl alcohol (25 : 24 : 1) mixed solvent. Dialysis was used to extract the water layer in the obtained sample. DNA and precipitation were performed using a 3 M solution of sodium acetate/ethanol (V/V = 1 : 20) overnight at −20 °C. The extracted DNA samples were dehydrated at room temperature in a vacuum oven and dissolved using TE buffer. Finally, the PicoGreen fluorescent dye and the Modulus detector were used to determine the content of the residual DNA.

2.3 Characterization of acellular matrix collagen content

The hydroxyproline detection kit produced by Sigma was used to measure the collagen content and was calculated by the amount of hydroxyproline. The dECM and untreated cartilage tissue was hydrolyzed using 6 M HCl at 120 °C of water for 3 h and cooled to 65 °C. Subsequently, 100 mL of chloramine *T* concentrate and oxidation buffer mixed solvent was added to the sample and incubated at room temperature for 5 min. An additional 100 mL of dimethylbenzaldehyde solution was added to each sample and then incubated for 90 min at 60 °C. An infinite M200 multifunctional microplate reader was used to read the absorbance at 560 nm and draw standard curves.

2.4 Characterization of the acellular matrix glycosaminoglycan content

Glycosaminoglycan content was measured using an aminoglycan sulfate assay kit from Biocolor, and dECM was digested with untreated cartilage tissue in 0.01 M HCl using pepsin (1 mg mL^{-1}). A 0.01 M HCl solution of pepsin was used as a control during testing.

2.5 Preparation of the anisotropic hydrogel

1 g of dECM fine powder was added in to 9 mL of a 15 mg mL^{-1} pepsin in 0.01 M HCl solution with a pepsin to mass ratio of 1 : 10. The suspension is stirred at room temperature for 48 h so that it is completely digested (with no visible powder) to form a flowable viscous solution. The viscous solution was adjusted to neutral with 0.1 M NaOH solution and 10× PBS, diluted with 0.01 M PBS at a particular dECM concentration, and stored at 0 °C for reserve.

The prepared pre-gel solution was divided into two parts; one added 1 mL of 2 mg mL^{-1} type II collagen as phase A. The other contains sucrose solution of different concentrations (1%∼3% w/v) to adjust the density and 5% w/v chitosan to adjust viscosity as phase B; 0.1 g sodium polyaldehyde alginate was used as the crosslinker. During preparation, 1 mL of phase A was added to the mold, and then 1 mL of phase B was injected into phase A. The two phases were quickly layered to form a layered structure. The mold was put into a 37 °C incubator, and the anisotropic hydrogel was obtained after a constant temperature for 10 min.

2.6 Characterization of the morphology of the anisotropic hydrogel

The as-prepared gels were frozen in liquid nitrogen, quenched, and lyophilized, and the resulting samples were gold-sprayed to observe their internal morphology at 5–15 KV using an electron scanning microscope.

To further observe its internal structure *in situ*, the resulting hydrogel was injected into specific copper molds, frozen with liquid nitrogen, and lyophilized using a cryo scanning electron microscope.

2.7 Characterization of the mechanical properties of the anisotropic hydrogel

The pre-gel solution was injected into a 1 cm × 1 cm × 5 cm Teflon mold and incubated for 30 min at 37 °C to complete the gelation. Samples were taken at various locations of the hydrogel sample and subsequently stretched at 1 mm min^{-1} until the sample broke. The hydrogel's compression modulus, loss modulus, and loss angle tangents were determined using a dynamic thermodynamic analyzer. Gel dynamics were detected using a rotary rheometer.

The hydrogel was immersed in PBS for 24 h, lyophilized, and the volume (V) of the scaffold sample was accurately measured. The mass of the dry sample (m_1) and the mass of the sample immersed in anhydrous ethanol after 2 h (m_2) were measured. The porosity (P) of the sample calculation formula is $P = [(m_2 - m_1)\rho]/V$.

2.8 Synthesis of the drug carrier

The synthesis of mesoporous silica was prepared by a modified Stober method, where 100 g water, 23.4 g ethanol, 0.8 mL of concentrated ammonia and 0.8 g trimethyl ammonium bromide were added to the flask, mixed for 30 min, and 5 mL of ethyl silicate for 35 °C for 24 h. The products were washed repeatedly with ethanol and then added to the sorter extractor by acetone for 72 h, lyophilized after washing, to obtain mesoporous silica particle dry powder.

The resulting 1 g of mesoporous silica was obtained by dispersing in 100 g of ethanol with 0.25 g of aminopropyl triethoxysilane, reacted for 12 h at 70 °C, and the product was washed with ethanol/distilled water (v/v = 1/1) to obtain the surface amino-modified drug carrier particles.

A certain amount of KGN was dissolved in DMSO, mixed with DMSO dispersion of the above carrier particles, and EDC/NHS catalyzed the condensation of amino and carboxyl groups. After reaction at room temperature, centrifugation, washed with distilled water, lyophilized to obtain mesoporous silica. The products were characterized using scanning electron microscopy, nitrogen adsorbent apparatus, zeta potential analysis, and infrared spectroscopy.

2.9 Loading of drug carriers and cells

1 mL of bone marrow-derived stem cells (5×10^5 cells per mL) and 1 mL of drug carrier (1% w/v) was mixed with 8 mL of the pre-gel solution (4 mL of phase A and 4 mL of phase B, the dECM concentration was 10 mg mL^{-1}). Subsequently, the cell-loaded hydrogel was obtained by injecting both cell-loaded pre-gel solution into 6-well culture plates for 30 min at 37 °C.

2.10 Characterization distribution of drug carriers and cells

Anisotropic hydrogel loaded with drug carrier was interrupted longitudinally after freezing using liquid nitrogen, EDS by scanning electron microscopy and scanning Si elements to obtain the gradient distribution of the drug carrier in the hydrogel.

The gradient distribution of cells in the hydrogel was observed in the cell-loaded anisotropic hydrogel after 15 min of fixation with paraformaldehyde, stained using DAPI dye and subsequently sectioned longitudinally and visualized using a laser confocal microscope.

2.11 *In vitro* cell toxicity and proliferation

The resulting hydrogel loaded with drug carriers and MSCs was added to the corresponding cell culture medium for continued culture, which was changed every two days. CCK-8 staining was performed to assess cell survival in dECM hydrogel. The numbers of viable and dead cells in the results were calculated separately, and cell viability was obtained by the number of viable cells/total cell number treatment.

2.12 qT-PCR

The resulting hydrogel loaded with drug carriers and MSCs was added to the corresponding cell culture medium for continued culture, which was changed every two days. Samples were also taken every other week to use qT-PCR for the expression levels of Col2A1, SOX9, Aggrecan, and GADPH concentrated as chondrogenic differentiation markers to characterize their ability to promote chondrogenic differentiation of mesenchymal stem cells.

2.13 Animal experiments

Twenty-four healthy adult male New Zealand white rabbits, 3 months old, weighing 2.5–3.0 kg were used. They were randomly divided into three groups: A, B, and C. All animal procedures were performed in accordance with the Guidelines for Care and Use of Laboratory Animals of Guangdong Provincial People's Hospital and approved by the Animal Ethics Committee of Guangdong Provincial People's Hospital. Laboratory animals were kept in common grade, all experimental

animals were kept under the same conditions, and all could move freely in the cage.

Group A: Experimental group, 8 animals, KGN and MSCs loaded anisotropic hydrogels were implanted at the defect position.

Group B: Control group, 8 animals, KGN and MSCs loaded isotropic hydrogels were implanted at the defect position.

Group C: Blank group, 8 animals, no hydrogels were implanted at the defect position.

Animal models of joint injury were prepared by drilling through the knee cartilage in New Zealand white rabbits. The median incision of about 3 cm was made in the rabbit knee joint, the subcutaneous fascia was separated, the medial femoral muscle was partially cut, the medial support band of the knee was cut, and the rabbit patella was turned laterally to expose the cartilage surface of the knee. Subsequently, in the middle of the rabbit knee joint, a circular osteochondral defect with a diameter of 3 mm was made at a depth of 4.5 mm. Saline was used for flushing the defect and the knee joint. The muscle tendon layer, subcutaneous fascia layer and skin layer were stitched successively, and sterile accessories were used to wrap the wound. After surgery, the penicillin solution was prepared with normal saline, and the experimental animals were injected intramuscularly at 400 000 units per time. The physiological state of the animal should be observed continuously after surgery. If infection and wound cracking occur, they should be treated in time.

The corresponding pre-gel solutions were separately injected into the cartilage damage in the animal model. After the completion of the gelation, the animals are fed for different periods. Before sacrifice, the experimental animals' physiological state and daily activities are continuously observed. Each group of experimental animals adopts the same feeding conditions and can move freely in the cage.

At weeks 4,8,12 and 16 after implantation, 10 mL of air was injected into the ear edge vein to cause air embolism to kill the experimental animals. Subsequently, the hydrogel and the surrounding tissues at the knee joint of the experimental animal model were isolated. The femoral condyle was stored in formalin solution and decalcified using an EDTA decalcification solution. Sections were followed by hematoxylin-eosin, toluidine blue staining and collagen II immunohistochemical staining, and observation using an inverted fluorescence microscope to evaluate the repair.

3 Results and discussion

3.1 Synthesis and characterization of decellularized extracellular matrix

A schematic illustration of the fabrication process of anisotropic hydrogel is shown in Fig. 1, including the morphology of cartilage, dECM, pre-gel solution and anisotropic hydrogel. The untreated cartilage is smooth with a white luster. After decellularization, the dECM present a white, chyme-like appearance. The pre-gel solution, which undergoes further digestion, is a viscous liquid. When the gelation is completed, the final product is an anisotropic hydrogel (one component is stained with methyl orange to indicate the gradient).

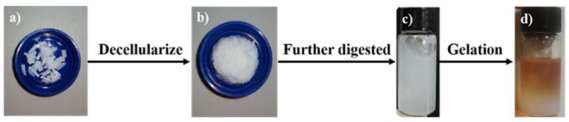

Fig. 1 Morphologies of (a) cartilage; (b) dECM; (c) pre-gel solution and (d) anisotropic hydrogel.

The dsDNA content detection kit was used to detect the DNA content in ECM and dECM (Fig. 2a–c). The results showed that the content of double-stranded DNA decreased from 118.35 ng mg^{-1} to 1.74 ng mg^{-1} by physical, chemical, and biological methods, avoiding the occurrence of immune reactions in subsequent animal experiments. Meanwhile, the mass fraction of collagen increased from 37.16% to 76.93%, and the content of glycosaminoglycan decreased from 14.85% to 2.19%. The original chemical components are basically maintained, and the decrease in glycosaminoglycan content may be caused by using SDS, which will be adjusted by adding the corresponding raw materials in the subsequent preparation process. In order to optimize the decellularization process, we improved the original decellularization method. We first treated cartilage tissue into paste through grinding and deep digestion and repeated the above physical, chemical, and biological methods, and the experimental process was monitored, and finally, the processing time was shortened to 15 h (Fig. 2d).

After embedding the cartilage tissue and acellular cartilage tissue, HE staining found that the purple nucleus disappeared in the cartilage tissue after decellularization, which proved the degree of decellularization (Fig. 3).

3.2 Synthesis and characterization of anisotropic hydrogel

After freezing-drying the products of each stage, samples were taken for observation under a scanning electron microscope, and cavities of about 10 μm appeared in the tissue after the

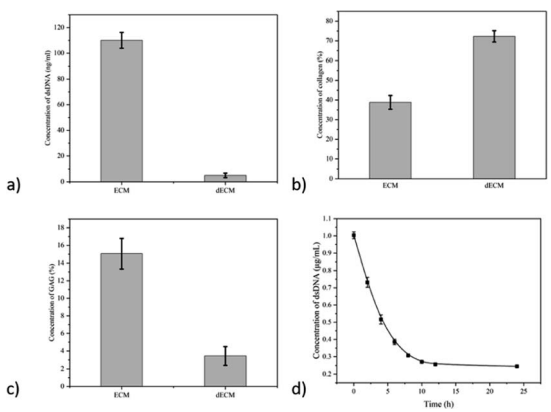

Fig. 2 Changes in the content of various components before and after decellularization of cartilage tissue: (a) dsDNA; (b) collagen; (c) GAG. And the concentration variation of dsRNA over time during decellularization.

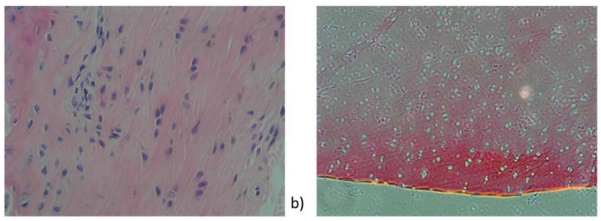

Fig. 3 HE-stained sections of cartilage tissue and acellularized cartilage tissue.

decellularization of the cartilage tissue (Fig. 4a). The decellularized extracellular matrix was deeply digested and reconfigured into a hydrogel with a uniform inner cavity size of about 20 μm (Fig. 4b).

The anisotropic structure of as-prepared hydrogel is fabricated by the controlled diffusion method. When two phases with different densities are mixed, due to the influence of buoyance (caused by the differences in density), the mixed pre-gel solution undergoes a phase separation to generate an anisotropic structure. To immobilize this structure, the solution was put under the 37 °C, after curing for 10 min, the gelation progress is finished and an anisotropic hydrogel is achieved. The final morphology and structure of the hydrogel can be easily tuned from gradient to A and B double layer and A–C triple layer with the adjustment of the pre-gel solution's viscosity and density.

To reduce the influence of the sample preparation procedure on the morphology characterization, the anisotropic hydrogel was frozen immediately after synthesis. The inner structure is directly observed using a cryo scanning electron microscopy *in situ*, and the result also confirms the directional distribution of pores in different locations (Fig. 4c and d).

Due to the critical role of cartilage tissue in physiological activities, the mechanical properties of implants have specific requirements, due to the poor original mechanical properties of the acellular matrix, the hydrogel is further crosslinked by adding a crosslinker (polyaldehyde alginate) to improve its mechanical properties.

The gelation time was first characterized by a rotary rheometer and found that the hydrogel was completed at about 13 min (800 s) at 37 °C after injecting the pre-gel solution into the mold, a data that met the requirements of subsequent animal experiments (Fig. 5a).

The mechanical properties of the products were further characterized using a dynamic thermodynamic analyzer, and due to the anisotropic properties obtained, the test was truncated into four parts of the gel along different heights. The test results show that the loss modulus of each segment is about 1.4 kPa, 0.81 kPa, 0.58 kPa, and 0.26 kPa; the energy storage modulus is about 3.13 kPa, 2.01 kPa, 1.69 kPa and 0.88 kPa (Fig. 5b and c).

The nature of the porosity can also be proved by measuring the porosity of the hydrogel. We also intercepted the four parts of the hydrogel using the ethanol method, and we saw that the porosity was 61.38%, 72.57%, 83.46%, and 91.24%, respectively (Fig. S2†).

The anisotropic hydrogels were fabricated by regulating the diffusion of pre-gel solutions and crosslinker solutions, and the product has the anisotropic chemical composition and physical properties, which have been confirmed. At the same time, we used the decellularized matrix as the raw material to ensure the low immune activity of the product and improved its mechanical properties by adding crosslinkers, laying a theoretical foundation for the following cell experiments and animal experiments.

3.3 Loading of KGN and cells onto the anisotropic hydrogel

Under the transmission electron microscope, mesoporous silica particles have a uniform size with a diameter of 200 nm and a pore diameter of about 3 nm. By Zeta potential test, the original mesoporous silica particle potential is −36 eV, with a positive surface charge after –NH_2 coupling modification, the Zeta potential rises to 28 eV, and the surface Zeta potential drops to −5 eV due to partial ammonia occupation of grafted KGN (Fig. 6a and b).

Since KGN itself is a hydrophobic drug, a drug carrier able to disperse in water should load it and be able to release it in physiological conditions. Therefore, mesoporous silica microspheres were selected as the drug carrier and modified using amino-terminated silane-coupled reagents to graft KGN to its surface by EDC/NHS. The grafting of KGN on the surface of

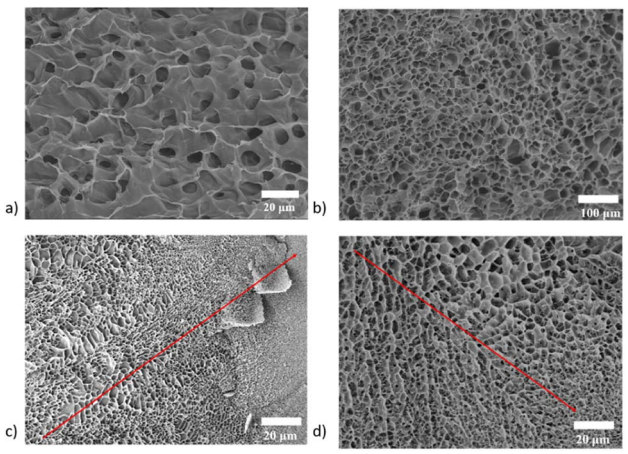

Fig. 4 SEM images of (a) decellularized extracellular matrix; (b) dECM hydrogel; (c and d) *in situ* cryoscanning electron microscopy of anisotropic hydrogel (inset arrow indicates the change of pole size through the axis).

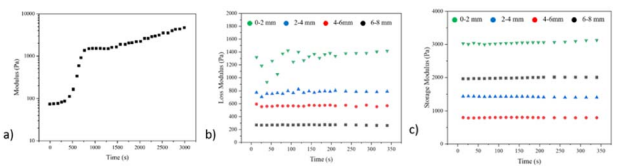

Fig. 5 (a) Gelling kinetics of anisotropic hydrogel; (b) loss modulus; (c) storage modulus from different locations of the anisotropic hydrogel.

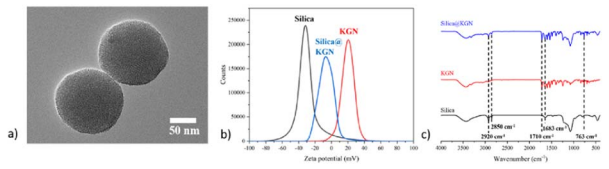

Fig. 6 (a) TEM images of mesoporous silica nanoparticles; (b) Zeta potential and (c) FTIR spectrum of mesoporous silica nanoparticles, modified mesoporous silica nanoparticles and the KGN loaded mesoporous silica nanoparticles.

mesoporous silica particles can also be demonstrated by infrared spectroscopy, as shown below. The peaks at 2920 cm^{-1} and 2850 cm^{-1} belongs to the C=C bond in the mesosphere silica, the peaks at 763 cm^{-1} belongs to the benzene in the KGN, the peaks at 1710 and 1683 cm^{-1} belongs to the C=O bond in KGN. Combining the information, the grafting of KGN onto the drug carrier is confirmed (Fig. 6c).

The critical point of this research is to prepare a hydrogel with anisotropic properties, thus requiring the distribution of internal drug carriers and cells. Since the Si element in the drug carrier is specific, due to its only source in the hydrogel is from the drug carrier, we scan the hydrogel using EDS and find that the content of the Si element generally decreases axial, which proves the distribution of the mesoporous silica microsphere in the hydrogel (Fig. 7a and b). Because the cartilage tissue itself has a laminar structure, the distribution of loaded MSCs should also be considered in the preparation process. After cutting the resulting cells-loaded anisotropic hydrogel along the longitudinal direction, staining with DAPI dye, and observing under a laser confocal microscope, the cell density also changed along the axis, further demonstrating the anisotropic nature of the gel (Fig. 7c and d).

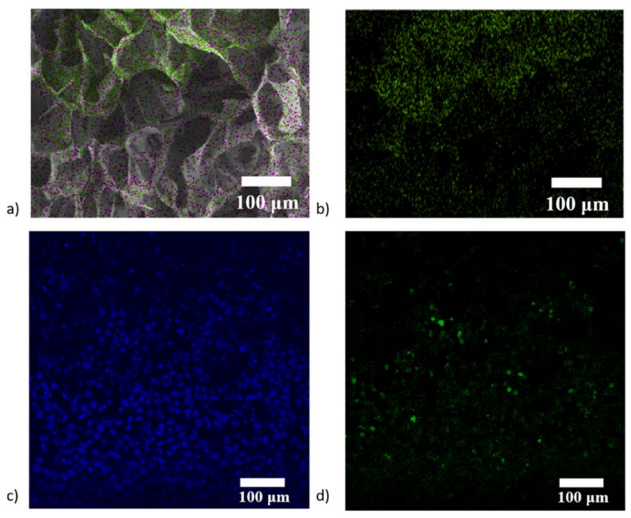

Fig. 7 (a and b) EDS spectrum of mesoporous silica nanoparticles loaded anisotropic hydrogels (green points shows the distribution of Si elements); (c and d) con-focal microscope images of DAPI stained cell loaded anisotropic hydrogel.

3.4 *In vitro* experiment

Based on the gradient distribution of the cells in the hydrogel, we sliced the hydrogel into four parts every 2 mm and monitored the proliferation level of the cells in these four parts separately. The specific testing method is CCK-8, and samples are taken every two days for 20 days.

By monitoring the level of cell proliferation, we found that the proliferation level gradually increased along the top to the bottom of the hydrogel, and the MSCs at the top of the hydrogel tend to have lower proliferation than those at the bottom of the hydrogel (Fig. 8)., since the amount of cell in the bottom is higher (Fig. 7c).

Biosafety and biological effectiveness are two essential components in the performance evaluation of biomaterials, so we used qPCR to examine the expression of chondrogenic differentiation markers of hydrogel MSCs at different periods. The results showed a 3.22-fold higher Col2A1 expression, 4.97-fold higher SOX9 expression, 3.16-fold higher Aggrecan expression, and 7.67-fold higher GADPH expression after 4 weeks of culture. It has been proved that this hydrogel can effectively promote the differentiation of mesenchymal stem cells to chondrocytes (Fig. 9). In conclusion, a drug carrier grafted with KGN was synthesized to promote the chondrogenic differentiation of MSCs. The gradient distribution of drug carriers and MSCs in the hydrogel was demonstrated. The possibility of an anisotropic hydrogel as a biological scaffold for cartilage tissue repair was verified.

3.5 *In vivo* experiment

All experiment animals received a regular diet and gained weight for at least 16 weeks after surgery. None of them had severe complications, such as death. All the experiment animals' incisions healed smoothly, and joints' activity was regular with good recovery. The skin and subcutaneous tissue were opened at the incision scar; no injection and surgery traces could be observed by the naked eye, and no adhesion, scar, tumor formation, swelling, and exudation in the injection area.

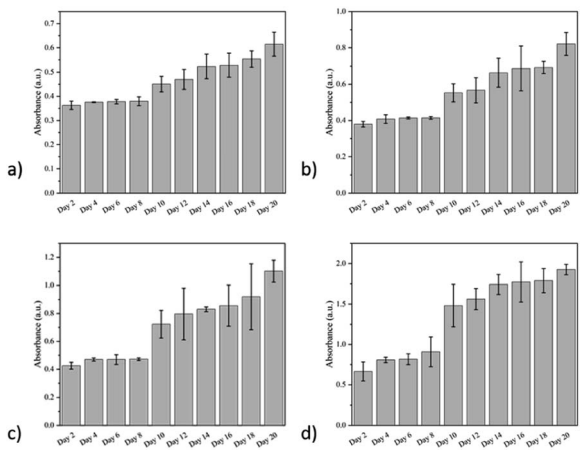

Fig. 8 Cell proliferation levels at different locations of the anisotropic hydrogel: (a) 0–2 mm; (b) 2–4 mm; (c) 4–6 mm; (d) 6–8 mm.

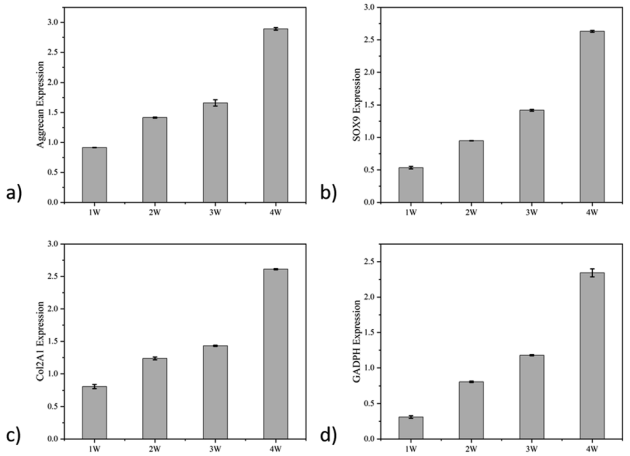

Fig. 9 The chondrogenic marker expression levels of the cells in different hydrogel layers: (a) aggrecan; (b) SOX 9; (c) Col2A1; (d) GADPH.

Rabbits were sacrificed at week 4, 8, 12, and 16. Samples were taken for the general obversion of each group's repair effect of the cartilage defect. At different time points of the animal experiment, the holes on the cartilage were clearly visible at 4 W, most of the holes were repaired, and by 16 W, a slight depression in the center of the damaged area. The current results in animal experiments demonstrate the potential of anisotropic hydrogel in cartilage damage repair (Fig. 10).

Mild hyperplasia of the synovial membrane in the knee joint and a small amount of synovial fluid in the joint was found in the week 4 sample, the articular surface cartilage defect is clearly visible, and a very slight amount of cartilage-like new tissue can be barely seen in the defect, the infillings show an appearance of uneven and concave (Fig. 10a). The intraarticular synovial membrane of the sample at week 8 also had mild edema, and the visual defect was still very obvious with a round and blunt convex edge, and the defect tissue was also presented as gray-white, with blurred boundary with the normal tissue

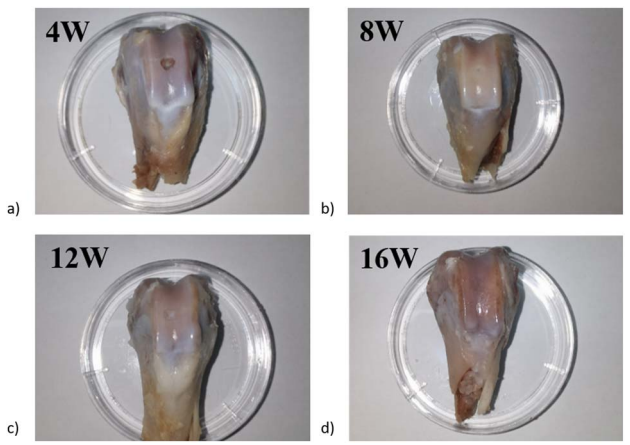

Fig. 10 Appearance of articular cartilage injury sample after different times of repair: (a) 4 weeks; (b) 8 weeks; (c) 12 weeks and (d) 16 weeks.

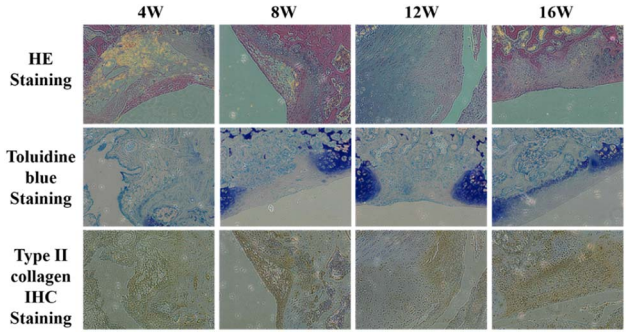

Fig. 11 Pathological staining images of the sample at 4, 8, 12 and 16 weeks.

(Fig. 10b). In week 12, the edema around the sample disappeared, the surface of the new tissue was still not smooth, and a slight concave was visible in the middle of the defect position; the boundary is barely distinguished from the surrounding normal tissue. The surface gloss is slightly better than the previous group, with similar transparent cartilage-like tissue, but the tissue coverage degree is about 80% (Fig. 10c). In the sample taken at 16th week, the infillings at defect tissue and surface smoothness were better than that of the other three groups, basically flush with the surrounding joint surface, the new tissue was white, with uniform color, gloss, higher integrity, and connection with the surrounding normal tissue, and the boundary was almost indistinguishable by the naked eye (Fig. 10d).

In HE staining of the samples at week 4, the cartilage defect area was uneven, and the surface was depressed. A slight amount of cell growth was visible by HE staining, and the GAG contents were presented by toluidine blue staining. Type II collagen immunostaining proved that collagen synthesis began at the scaffold implantation.

As for samples taken at week 8, HE staining and toluidine blue staining already showed more cells and glycosaminoglycans on the surface layer of the defect, with a filling coverage of about 40%. The synthesis level of type II collagen is also increasing. By week 12, the defect position was completely filled, and HE staining and toluidine blue staining demonstrated that cells were already heavily present in the defect. Furthermore, the glycosaminoglycans at the defect position start to increase, together with the massive synthesis of type II collagen confirmed by immunohistochemical staining, demonstrating that the repair of the injury was nearly ended. By week 16, HE staining demonstrated a large distribution of cells at the injury site. Toluidine blue staining demonstrated that glycosaminoglycans began to deposit in the defect and that collagen type II was sufficiently expressed in the defect, demonstrating that the repair of the defect was complete (Fig. 11).

4 Conclusions

We designed and prepared an anisotropic scaffold based on a pig-derived acellular matrix and characterized their various physicochemical properties. Mesoporous silica nanoparticles

loaded with KGN for the sustained release of KGN are fabricated and dispersed in the scaffold, together with MSCs. The anisotropic feature is confirmed by multiple characterizations (SEM, EDS, CLSM, *etc.*), proving the gradient nature of the hydrogel. The toxicity of the as-prepared hydrogel is negligible, and the hydrogel can promote the chondrogenic differentiation of MSCs. Finally, rabbits were chosen as animal models. After implanting the anisotropic hydrogel for a while, sacrificing the experimental animals for further HE staining, toluidine blue staining, and collagen II immunohistochemical staining, the final pathological results show that the anisotropic hydrogel is capable of utilizing as a biological scaffold or the repair of cartilage damage. The excellent performance of the anisotropic hydrogel lays a foundation for further clinical application and mechanism research.

Ethical statement

All animal procedures were performed in accordance with the Guidelines for Care and Use of Laboratory Animals of Guangdong Provincial People's Hospital and approved by the Animal Ethics Committee of Guangdong Provincial People's Hospital.

Author contributions

The manuscript was written through contributions of all authors. All authors have given approval to the final version of the manuscript.

Conflicts of interest

There are no conflicts to declare.

Acknowledgements

This work was supported by the Natural Science Foundation of Guangdong Province (2022A1515011306, 2020A1515010268, 2021A1515011008), the Outstanding Young Talents Foundation of Guangdong Provincial People's Hospital (KJ012019091), the Program of Science and Technology of Guangzhou (202103020166, 201904010424, 202102020924, 202201011229), NSFC Incubation Project of Guangdong Provincial People's Hospital (KY0120220031), the Fundamental Research Funds for the Central Universities(2020ZYGXZR010). We encourage the citation of primary research over review articles, where appropriate, in order to give credit to those who first reported a finding. Find out more about our commitments to the principles of San Francisco Declaration on Research Assessment (DORA).

References

1 E. A. Makris, P. Hadidi and K. A. Athanasiou, *Biomaterials*, 2011, **32**, 7411–7431.
2 L. J. Reckers, D. J. Fagundes and M. Cohen, *Knee*, 2009, **16**, 290–294.
3 H. H. Lu and S. Thomopoulos, *Annu. Rev. Biomed. Eng.*, 2013, **15**, 201–226.
4 P. B. Messersmith, *Science*, 2008, **319**, 1767–1768.
5 F. Ulloa and J. Briscoe, *Cell Cycle*, 2007, **6**, 2640–2649.
6 P. Garrison, S. Yue, J. Hanson, J. Baron and J. C. Lui, *PLoS one*, 2017, **12**, e0176752.
7 V. Vogel and M. Sheetz, *Nat. Rev. Mol. Cell Biol.*, 2006, **7**, 265–275.
8 H. L. Ashe and J. Briscoe, *Development*, 2006, **133**, 385–394.
9 R. D. Singh, M. L. Hillestad, C. Livia, M. Li, A. E. Alekseev, T. A. Witt, P. G. Stalboerger, S. Yamada, A. Terzic and A. Behfar, *Tissue Eng. Part A*, 2019, **25**, 145–158.
10 X. Zhang, X. Gao, L. Jiang and J. Qin, *Langmuir*, 2012, **28**, 10026–10032.
11 L. G. Bracaglia, B. T. Smith, E. Watson, N. Arumugasaamy, A. G. Mikos and J. P. Fisher, *Acta Biomater.*, 2017, **56**, 3–13.
12 K. A. Mosiewicz, L. Kolb, A. J. van der Vlies, M. M. Martino, P. S. Lienemann, J. A. Hubbell, M. Ehrbar and M. P. Lutolf, *Nat. Mater.*, 2013, **12**, 1072–1078.
13 C. Li, J. P. K. Armstrong, I. J. Pence, W. Kit-Anan, J. L. Puetzer, S. Correia Carreira, A. C. Moore and M. M. Stevens, *Biomaterials*, 2018, **176**, 24–33.
14 *Neutrophil Methods and Protocols*, ed. M. T. Quinn and F. R. DeLeo, Humana Press, Totowa, NJ, 2014, vol. 1124.
15 R. J. Britten and R. B. Roberts, *Science*, 1960, **131**, 32–33.
16 L. Bai, X. Ma, J. Liu, X. Sun, D. Zhao and D. G. Evans, *J. Am. Chem. Soc.*, 2010, **132**, 2333–2337.
17 V. Parameswaran and A. Shukla, *J. Mater. Sci.*, 2000, **35**, 21–29.
18 J. T. Beals and M. S. Thompson, *J. Mater. Sci.*, 1997, **32**, 3595–3600.
19 J. M. Singelyn, J. A. DeQuach, S. B. Seif-Naraghi, R. B. Littlefield, P. J. Schup-Magoffin and K. L. Christman, *Biomaterials*, 2009, **30**, 5409–5416.
20 P. M. Crapo, T. W. Gilbert and S. F. Badylak, *Biomaterials*, 2011, **32**, 3233–3243.
21 T. W. Stapleton, J. Ingram, J. Katta, R. Knight, S. Korossis, J. Fisher and E. Ingham, *Tissue Eng. Part A*, 2008, **14**, 505–518.
22 J. M. Singelyn and K. L. Christman, *J. Cardiovasc. Transl. Res.*, 2010, **3**, 478–486.
23 J. M. Singelyn, P. Sundaramurthy, T. D. Johnson, P. J. Schup-Magoffin, D. P. Hu, D. M. Faulk, J. Wang, K. M. Mayle, K. Bartels, M. Salvatore, A. M. Kinsey, A. N. DeMaria, N. Dib and K. L. Christman, *J. Am. Coll. Cardiol.*, 2012, **59**, 751–763.
24 T. Yamasaki, M. Deie, R. Shinomiya, Y. Izuta, Y. Yasunaga, S. Yanada, P. Sharman and M. Ochi, *J. Biomed. Mater. Res.*, 2005, **75**, 23–30.
25 T. Yamasaki, M. Deie, R. Shinomiya, Y. Yasunaga, S. Yanada and M. Ochi, *Artif. Organs*, 2008, **32**, 519–524.
26 C. Scotti, A. Pozzi, L. Mangiavini, F. Vitari, F. Boschetti, C. Domeneghini, G. Fraschini and G. M. Peretti, *Knee Surg. Sports Traumatol. Arthrosc.*, 2009, **17**, 645–651.
27 Y. Duan, Z. Liu, J. O'Neill, L. Q. Wan, D. O. Freytes and G. Vunjak-Novakovic, *J. Cardiovasc. Transl. Res.*, 2011, **4**, 605–615.

28 M. T. Wolf, K. A. Daly, E. P. Brennan-Pierce, S. A. Johnson, C. A. Carruthers, A. D'Amore, S. P. Nagarkar, S. S. Velankar and S. F. Badylak, *Biomaterials*, 2012, **33**, 7028–7038.
29 M. J. Sawkins, W. Bowen, P. Dhadda, H. Markides, L. E. Sidney, A. J. Taylor, F. R. A. J. Rose, S. F. Badylak, K. M. Shakesheff and L. J. White, *Acta Biomater.*, 2013, **9**, 7865–7873.
30 D. O. Freytes, J. Martin, S. S. Velankar, A. S. Lee and S. F. Badylak, *Biomaterials*, 2008, **29**, 1630–1637.
31 J. S. Lee, J. Shin, H.-M. Park, Y.-G. Kim, B.-G. Kim, J.-W. Oh and S.-W. Cho, *Biomacromolecules*, 2014, **15**, 206–218.
32 C. J. Medberry, P. M. Crapo, B. F. Siu, C. A. Carruthers, M. T. Wolf, S. P. Nagarkar, V. Agrawal, K. E. Jones, J. Kelly, S. A. Johnson, S. S. Velankar, S. C. Watkins, M. Modo and S. F. Badylak, *Biomaterials*, 2013, **34**, 1033–1040.
33 C. Quint, Y. Kondo, R. J. Manson, J. H. Lawson, A. Dardik and L. E. Niklason, *Proc. Natl. Acad. Sci. U. S. A.*, 2011, **108**, 9214–9219.
34 J. A. DeQuach, S. H. Yuan, L. S. B. Goldstein and K. L. Christman, *Tissue Eng. Part A*, 2011, **17**, 2583–2592.